Nanoporous glass membranes fabricated by femtosecond laser micromachining for in vitro Lab-on-Chip applications

F. Torre*[a], A. Nardini[b,c], L.Cherubin[d], C. Conci[d], M.T. Raimondi[d], R. Osellame[b], A. Valente[a], R. Martínez Vázquez[b]

[a]Institute of Systems and Technologies for Sustainable Production (ISTePS), University of Applied Sciences and Arts of Southern Switzerland (SUPSI), via La Santa 1, 6962, Lugano, Switzerland, [b]Institute for Photonics and Nanotechnologies - National Research Council (IFN - CNR), Piazza Leonardo da Vinci 32, 20133 Milan (MI), Italy, [c]Department of Experimental Medicine - Università del Salento c/o College Isufi, Centro Ecoteckne, Via Monteroni 73100. Lecce, Italy, [d]Dept. of Chemistry, Materials and Chemical Engineering "Giulio Natta" - Politecnico di Milano, Piazza Leonardo da Vinci 32, 20133 Milan (MI), Italy

*federica.torre@supsi.ch, Phone: +39 3284158344

ABSTRACT

Developing effective treatments for neurodegenerative diseases such as Alzheimer's requires advanced in vitro models that accurately replicate physiological barriers like the blood-brain barrier (BBB). Lab-on-chip (LOC) platforms offer powerful tools to mimic these complex biological interfaces, enabling precise study disease mechanisms and evaluating therapeutic strategies. To effectively simulate the BBB, membranes with pore sizes in the range of a few hundred of nanometers are essential to ensure selective permeability and sterility.

In this context, glass-based membranes integrated into LOC devices provide superior chemical stability, biocompatibility, and optical clarity compared to conventional polymers, which suffer from molecule absorption and autofluorescence. However, fabricating nanoscale features in glass presents significant challenges.

To address this, we employ femtosecond laser irradiation combined with wet chemical etching. Through a fine tuning of the irradiation parameters, combined with a tight focusing condition, enables the fabrication of sub- 400 nm diameter through-holes after selective etching in NaOH of the modified regions. This approach allows nanoscale machining beyond traditional ultrafast laser micromachining limits.

The membranes pores size and homogeneity will be optically and morphologically characterized. Their permeability performance will be assessed through gas permeability tests using a two-chamber custom made sealed device. To validate biocompatibility and functionality, 3D cellular scaffolds will be fabricated via two-photon polymerization (2PP) directly onto the membrane surface.

This glass membranes offers a reliable, biocompatible, and optically transparent solution for LOC and biosensing applications requiring precise molecular filtration and sterile separation.

Keywords: BBB LOC, blood brain barrier, femtosecond processes, glass, silica, lab-on-chip, membrane.

Laser Applications in Microelectronic and Optoelectronic Manufacturing (LAMOM) XXXI, edited by Godai Miyaji, Gwenn Pallier, Nirmala Kandadai, Proc. of SPIE Vol. 13880, 1388009 · 2026 Published by SPIE
0277-786X · doi: 10.1117/12.3079803

1. INTRODUCTION

The blood–brain barrier (BBB) is a highly specialized vascular interface that regulates the exchange of molecules between the bloodstream and the central nervous system of human brain. Its restrictive function arises primarily from brain microvascular endothelial cells (BMECs), which feature tight junctions, polarized transport systems, and are supported by pericytes, astrocytes, and the basement membrane microenvironment. Traditional in vitro BBB models have historically relied on Transwell systems, but these approaches lack physiological shear stress, dynamic biochemical cues, and often fail to replicate the complexity of in vivo barrier properties. To address these limitations, a broad range of microfluidic BBB-on-chip platforms has emerged over the last decade.

Early microfluidic BBB models showed that perfusion-based architectures enable controlled analysis of trans-barrier transport, once endothelial cells have established a functional tight-junction network on the underlying synthetic membrane. For example, Griep *et al*. [1] developed one of the first BBB-on-chip devices incorporating shear stress and inflammatory modulation to evaluate endothelial barrier permeability under controlled microenvironmental conditions. Subsequent devices rapidly incorporated more sophisticated sensing modules. Kai-Hong Tu et al. [2] introduced real-time transendothelial electrical resistance (TEER) monitoring within an integrated microfluidic BBB model, enabling continuous quantification of barrier integrity rather than end-point measurements. Similarly, Yang *et al*. [3] proposed an "inoculate-first, assemble-later" strategy to improve reproducibility in BBB-on-chip platforms, addressing the variability caused by perfusion-based seeding in assembled devices. In their method, endothelial cells and astrocytes are sequentially cultured on opposite sides of a porous membrane prior to chip assembly, ensuring highly consistent cell densities and enabling clean integration with an independent TEER detection module.

Parallel work by Bonakdar *et al*. [4] introduced a microfluidic BBB model to study of permeability behaviour under pulsed electric fields, highlighting the utility of organ-on-chip systems in studying dynamic perturbations of the barrier. In their system, permeability is quantified optically by tracking diffusion of fluorescent tracers across hCMEC monolayers cultured on a permeable membrane, enabling real-time assessment of both reversible and irreversible electroporation regimes.

More recently, multiplexed and high-throughput BBB-on-chip architectures have been demonstrated. Techniques for parallelization allow simultaneous testing of multiple conditions or compounds, as shown by efforts such as the multiplexed BBB organ-on-chip platform which allows to perform eight different experimental conditions [5]. In parallel, comprehensive reviews have critically analyzed the growing landscape of BBB microfluidic models. Corral-Nájera et al. [6] provided a comprehensive overview of the wide range of membranes employed in organ-on-chip systems, covering commercial polymeric filters, engineered synthetic membranes, and biologically derived ECM-based interfaces. Their review highlights how membrane material, porosity, thickness, and surface chemistry critically shape barrier formation, cell–matrix interactions, and the resulting molecular transport properties. More recently, the extensive review underlined key challenges still limiting the field: lack of standardization in membrane characterization, variability in cellular sources, inconsistent reporting of permeability metrics, and the difficulty of isolating physical contributions of the chip from biological ones [7].

A recurrent observation across BBB-on-chip studies is that barrier function emerges from the coupled contribution of biological and physical components, yet the physical interface—the membrane and the microchannel architecture—is generally treated as a passive background element. Most platforms employ commercially available PET or PC membranes with pore sizes of 0.2–0.4 μm and thicknesses of 8–20 μm, originally designed for conventional Transwell assays rather than for mimicking the nanoscale selectivity of the in vivo endothelial tight-junction network [6,7]. In these systems, TEER and permeability readouts are commonly corrected by subtracting an acellular baseline measurement representing the electrolyte-filled membrane and channel resistance, so that only the cellular contribution is retained [8,9,10]. As a result, the physical barrier is conventionally removed from the analysis rather than examined as a controllable transport-modulating subsystem.

This gap suggests an opportunity for engineered tunable acellular barriers that mimic the physical selectivity of the BBB independently of cellular components. Such systems could serve as (i) standardized and reproducible baselines for interpreting biological chip data, (ii) platforms for dissecting how nanoscale geometry influences passive transport, and (iii) tools for pre-screening molecules based on fundamental permeability before deploying complex, slow, and variable cell-based models. Recent developments in femtosecond-laser microfabrication and precision nanostructuring now enable the creation of ultra-thin inorganic membranes with sub-micrometric pores and tightly controlled porosity—properties that cannot be achieved with standard polymeric membranes.

In this work, we build upon the limitations identified in current BBB-on-chip systems and propose a physically defined, acellular barrier platform based on laser-nanostructured inorganic membranes. By isolating and quantifying the purely physical component of transport—decoupled from cellular variability—this approach aims to complement existing biological BBB models and offer a reproducible foundation for next-generation BBB-on-chip technologies.

2. DESIGN

2.1 Membrane design

The aim of this work is to manufacture a glass-based permeable membrane. The objective is to have a glass substrate in the order of hundred of micrometre thickness perforated throughout all its depth by a squared pattern of defect-free holes distanced tents of microns.

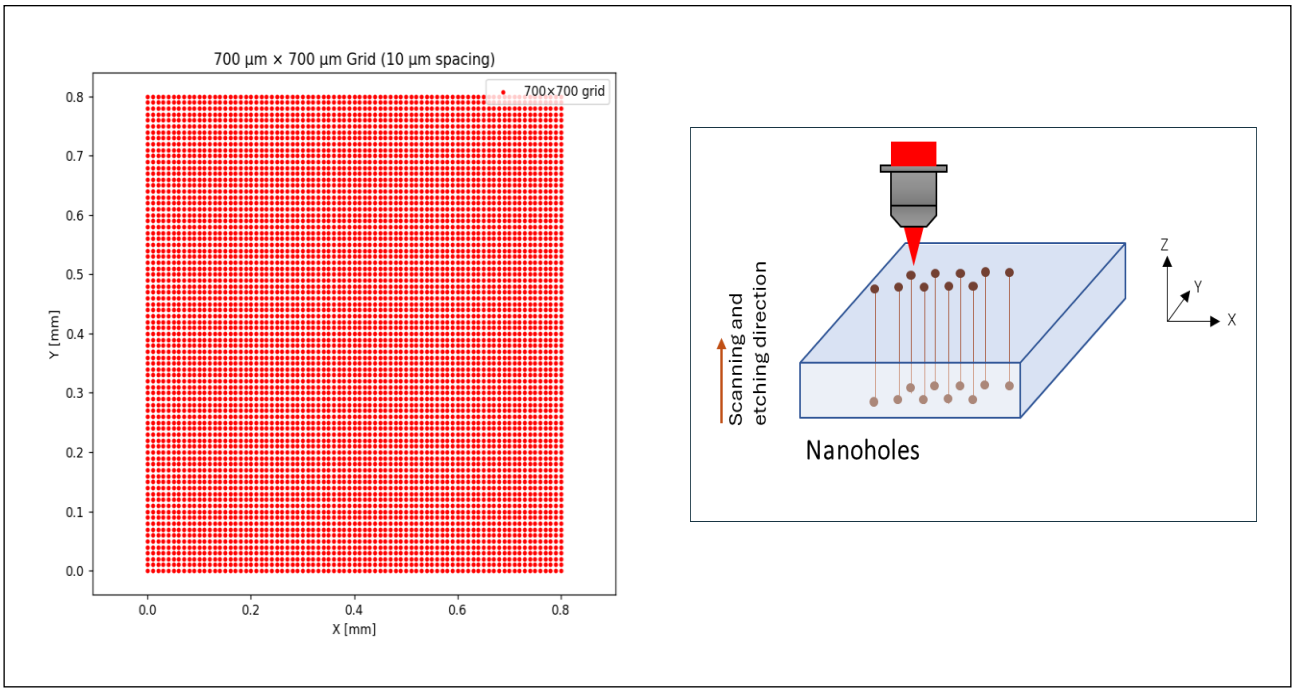

Figure 1 Schematic illustration of the nanoporous membrane design and laser scanning strategy. The square pore array (700 × 700 µm) defines the membrane active area, while the three-dimensional view illustrates the axial laser writing trajectory through the glass substrate during selective laser etching.

2.2 Microfabrication process

In our study we used a two step process defined as Selective Laser Etching (SLE). SLE is a microfabrication technique that enables the creation of three-dimensional structures with micrometric resolution inside transparent materials such as fused silica, borosilicate or quartz. The method relies on the combination of (i) localized material modification induced by tightly focused ultrashort laser pulses and (ii) a chemical etching of the modified regions. This approach provides unique advantages for producing high-aspect-ratio nano/microstructures—such as the sub-micrometric pores required for biomimetic barrier membranes—while maintaining high geometric fidelity and mechanical stability.

In the first step, femtosecond laser pulses are focused inside the bulk of the glass substrate, inducing a localized change of material properties within the focal volume. The interaction is driven by nonlinear absorption processes, including multi-photon absorption and avalanche ionization, which collectively lead to the formation of a laser-modified region (LMR). Depending on the irradiation conditions, the LMR may exhibit changes in density, refractive index, birefringence.

The morphology and size of the LMR strongly depend on laser parameters such as pulse energy, repetition rate, numerical aperture of the focusing objective, scanning velocity, and polarization.

Chemical etching is usually performed with potassium hydroxide (KOH), sodium hydroxide (NaOH), and hydrofluoric acid (HF). While HF provides high etching rates, KOH and NaOH are often preferred due to superior selectivity and safer handling, especially at elevated temperatures.

For the fabrication of sub-micrometric pores, SLE offers significant advantages, nanometric control over pore geometry is inherited from the laser writing stage, allowing highly reproducible pore diameters, spacing, and orientation.

In the context of this work, SLE provides the necessary precision to engineer reproducible inorganic membranes with sub-micrometric pores, enabling the systematic investigation of the physical component of molecular transport across well-defined geometries. The ability to tune pore diameter and density while maintaining stable mechanical properties makes SLE-fabricated membranes a promising platform for generating controlled, acellular analogues of the blood–brain barrier.

3. MATERIAL AND METHODOLOGY

3.1 Material selection and holder design

Sub-micrometer pores were fabricated inside 170 µm-thick silica glass substrates through a two-step process involving femtosecond laser modification followed by alkaline chemical etching. The target pore dimension was kept in the sub-micrometric regime, with an average pore diameter of a few hundred nanometers, arranged in a regular 10 µm lattice pitch to enable future scaling toward millimeter-square membrane areas. The pores were designed to fully penetrate the substrate thickness, forming a permeable glass membrane suitable for physical transport studies (see Figure 1).

The glass substrate was mounted on a custom-designed holder integrated into the laser micromachining setup. The holder was designed to support the glass sample while allowing the circulation of water both above and below the substrate. This configuration ensured continuous immersion of the sample during laser inscription, while keeping the top surface fully accessible to the focusing optics of the water-immersion objective, as shown in Figure 2.

3.2 UPS laser equipment

Laser modification was performed using a femtosecond laser source (Light Conversion, Vilnius, Lithuania) emitting pulses with a duration of 167 fs at a central wavelength of 1030 nm. The repetition rate was varied between 10 and 100 kHz depending on the experimental conditions. Prior to laser inscription, the fundamental wavelength was frequency-doubled to 515 nm by second-harmonic generation.

The laser beam was focused inside the substrate using a 100X water-immersion objective (Nikon) with a numerical aperture of NA = 1.1. During laser inscription, the sample was mounted on Aerotech motorized translation stages. All laser modifications were performed at a fixed depth from the bottom surface of the substrate and along a constant writing direction.

Laser pulse energy was systematically varied in the range from 20 to 120 nJ, while the scanning speed was adjusted between 0.1 and 1 mm/s, allowing exploration of the parameter space relevant to selective laser etching and pore formation.

3.3 Laser writing strategy for SLE technology

To investigate how the laser–glass interaction affects pore continuity and subsequent chemical etching, two distinct laser writing strategies were implemented, as shown in Figure 2.

In the first configuration, the laser beam was continuously irradiated along the entire axial trajectory, crossing both glass–water interfaces. This approach was designed to maximize the continuity of the laser-modified region along the full substrate thickness.

In the second configuration, laser irradiation was interrupted approximately 3 μm before reaching the upper glass surface, with the aim of limiting stress accumulation at the glass–water interface while preserving axial continuity of the modified region.

This approach was further extended by turning off the laser approximately 15 μm before the top and bottom surfaces to minimize near-surface effects and to account for the finite response time of the laser modulation during axial scanning.

The laser-modified regions produced by each writing strategy were subsequently evaluated in relation to their compatibility with different chemical etching conditions, including both alkaline (NaOH) and hydrofluoric acid (HF) based processes, with the aim of identifying fabrication regimes suitable for robust and biologically compatible membrane fabrication.

3.4 Chemical etching after laser exposure

Following laser exposure, samples were chemically etched in a freshly prepared ≈1 M NaOH solution maintained at 60 °C (±0.5 °C). Samples were immersed for 2 h under mild agitation to promote homogeneous etchant diffusion along the full pore depth.

The resulting pore quality was assessed by optical microscopy, scanning electron microscopy (SEM), and a semi-quantitative scoring system evaluating pore opening completeness and the presence of structural defects such as cracks. This scoring approach enabled a systematic comparison between the different writing strategies and etching outcomes.

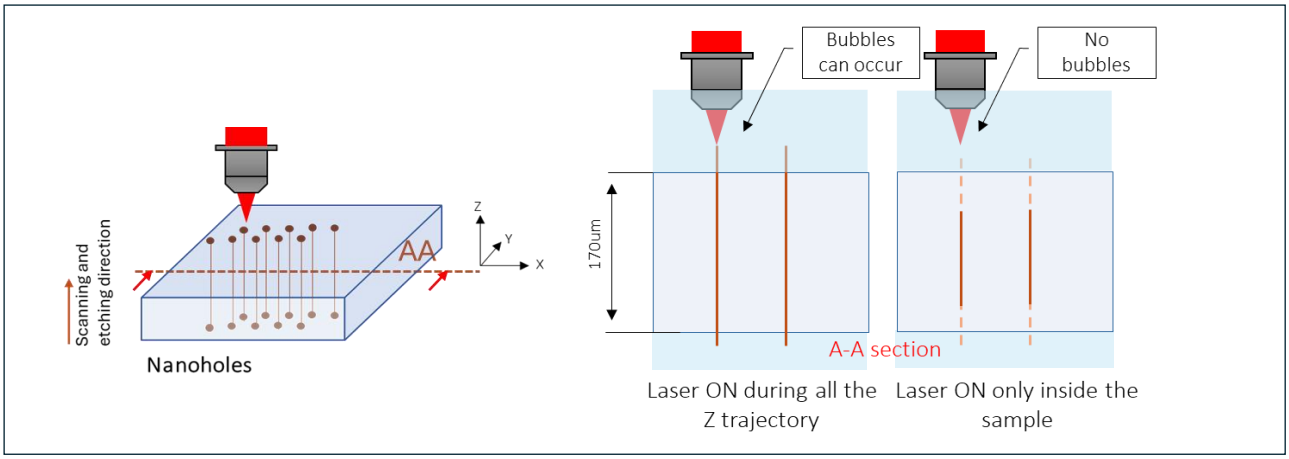

Figure 2 Schematic representation of the laser writing strategies adopted for selective laser etching. Continuous axial writing crosses both glass–water interfaces, whereas interrupted writing switches off the laser before reaching the interfaces to reduce near-surface stress accumulation.

4. RESULTS AND DISCUSSION

4.1 Effect of laser writing strategy on pore continuity and crack formation

The effect of laser writing strategy on pore dimension, morphology and crack formation was investigated by comparing different axial irradiation configurations aimed at modifying the laser–glass interaction near the glass–water interfaces. Scanning electron microscopy (SEM) and optical microscopy were as used to evaluate pore continuity, near-surface homogeneity, and the presence of structural defects following chemical etching.

Continuous axial writing, in which the laser beam intersected both glass–water interfaces, produced laser-modified regions with high axial continuity across the entire substrate thickness. At elevated pulse energies (Figure 4), this configuration resulted in the formation of complete etched holes with dimeter under the micron, but with near-surface defects, including microbubble formation and crack initiation, predominantly localized at the interfaces, indicating the onset of stress accumulation during laser exposure.

To reduce interface-related damage, interrupted writing strategies were explored by switching off the laser a few micrometres before the surface. At a pulse energy of 30 nJ, interrupting the laser approximately 15 µm before the interface led to a marked reduction in near-surface defects (Figure 3a). However, SEM analysis revealed the presence of extended unmodified regions close to the surface, resulting in poor pore homogeneity and incomplete opening after alkaline etching.

At the same pulse energy, reducing the interruption distance to approximately 3 µm improved the axial continuity of the laser-modified region (Figure 3b). Nevertheless, crack formation was still observed, indicating that stress-related defects were not fully suppressed by geometrical modification of the writing strategy alone. These observations highlight a trade-off between near-surface preservation and axial continuity, which persists even at low pulse energies.

Overall, the comparison between interrupted writing strategies demonstrates that variations in axial laser writing primarily affect pore homogeneity and continuity but are not sufficient on their own to fully eliminate crack formation. This suggests that additional parameters governing the laser–glass interaction, beyond the writing geometry, play a dominant role in determining pore integrity.

The influence of pulse energy on crack suppression is therefore systematically investigated in the following section.

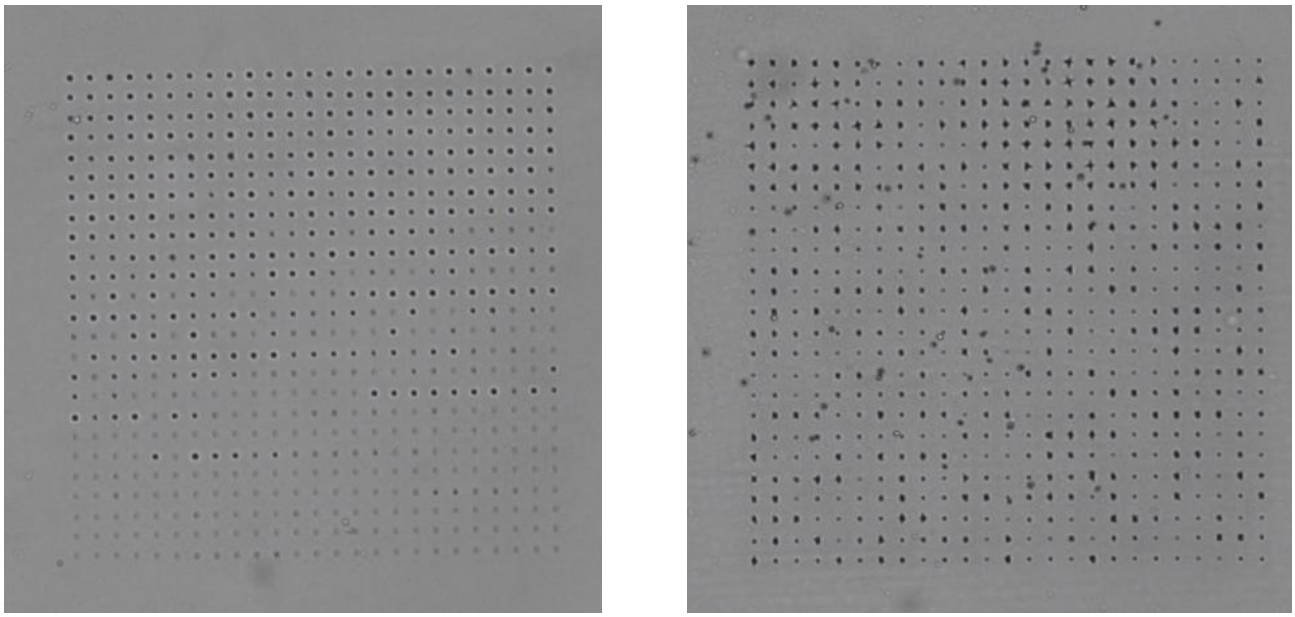

Figure 3 SEM images of pores fabricated at 50 nJ, scanning speed 0.5 mm/s, and repetition rate 25 kHz using interrupted laser writing strategies.
(a) Laser switched off ~15 µm before the upper surface (HF 5 min + NaOH 1 h).
(b) Laser switched off ~3 µm before the upper and lower surfaces (HF 1 min + NaOH 1 h).
Reducing the interruption distance improves axial continuity but does not fully suppress crack formation.

4.2 Role of laser pulse energy on crack suppression, etching accessibility, and pore size

Following the analysis of laser writing strategies, the influence of laser pulse energy on pore integrity was systematically investigated. Continuous axial writing was adopted while progressively reducing the pulse energy, and pore morphology was evaluated after chemical etching by scanning electron microscopy.

At high pulse energies (≥90 nJ), pore arrays were readily opened after etching; however, SEM inspection consistently revealed the presence of stress-induced defects, typically appearing as star-shaped cracks localized around individual pores (see Figure 4). These features indicate that, in this regime, the laser–glass interaction induces excessive localized stress, which is subsequently released during chemical etching.

Reducing the pulse energy resulted in a progressive suppression of crack formation. In the intermediate energy range (approximately 80–70 nJ), a marked decrease in crack density and severity was observed while maintaining effective pore opening with a diameter under the micron.

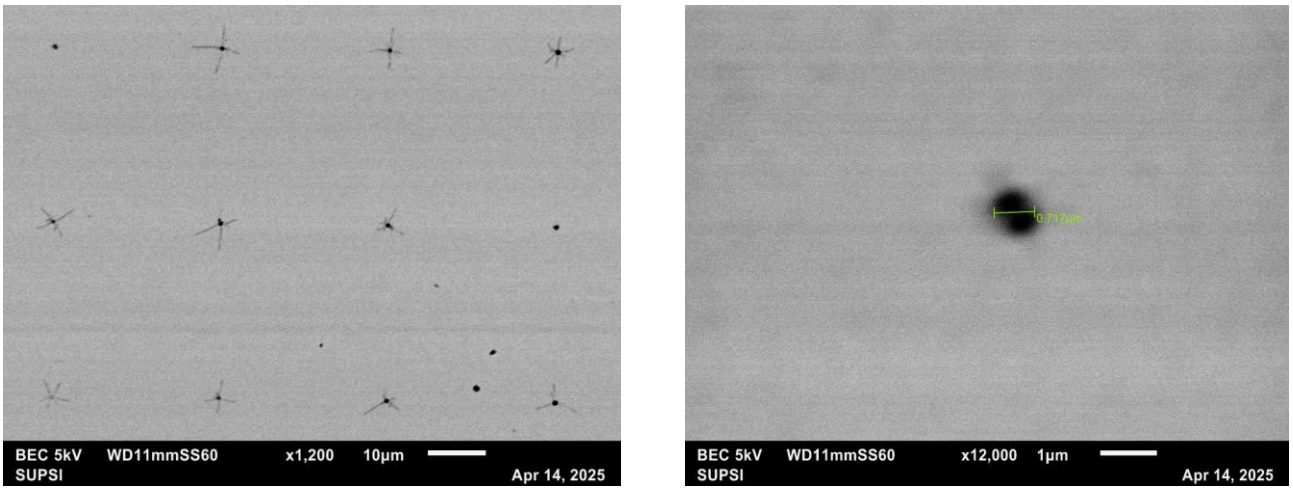

Figure 4 SEM images of pores fabricated by continuous axial laser writing at high pulse energy (120 nJ), scanning speed 1 mm/s, and repetition rate 10 kHz. Complete pore opening is achieved; however, pronounced near-surface defects, including microbubble formation and crack initiation, are observed at the glass–water interfaces.

However, SEM inspection revealed that pores fabricated in this regime exhibited irregular shapes and characteristic dimensions approaching the micrometre scale.

These observations indicate that, although stress accumulation at the glass–water interfaces is partially mitigated in this energy range, the extent of laser-induced modification remains excessive, leading to enlarged and poorly defined pore geometries. As a result, this regime represents a transition region rather than an optimal fabrication window for producing geometrically controlled, sub-micrometric pores (Figure 5).

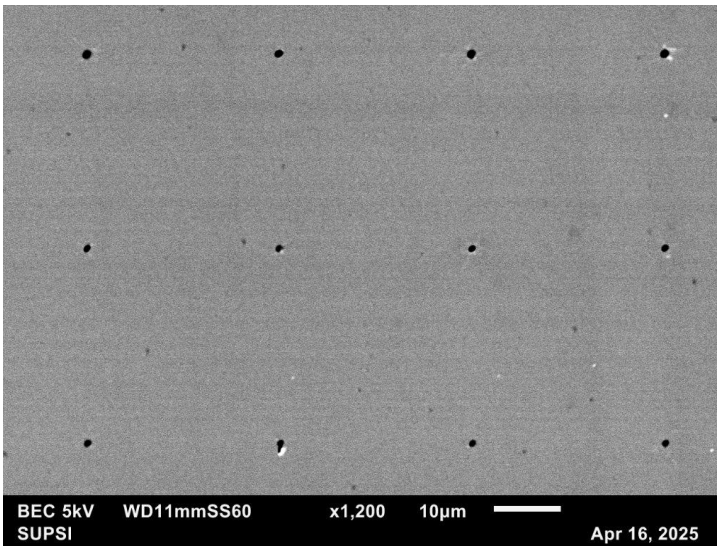

Figure 5 SEM images of pores fabricated at intermediate pulse energy (80 nJ), scanning speed 0.5 mm/s, and repetition rate 25 kHz after NaOH etching. Pores are opened with reduced crack density, but exhibit irregular shapes and micrometre-scale dimensions.

Further reduction of pulse energy identified a stable fabrication window between approximately 30 and 20 nJ. Within this range, continuous axial writing produced pores with strongly reduced or absent crack formation, while maintaining sufficient laser-induced modification to enable complete pore opening by alkaline etching alone. This regime therefore represents an optimal compromise between stress mitigation and etching accessibility.

High-magnification SEM (Figure 6) images acquired within this optimized energy window revealed that the fabricated pores exhibited sub-micrometric diameters, typically in the order of a few hundred nanometers. This pore size range is consistent with the targeted membrane design and confirms that selective laser etching enables the fabrication of nanoporous glass membranes with geometrically defined pores.

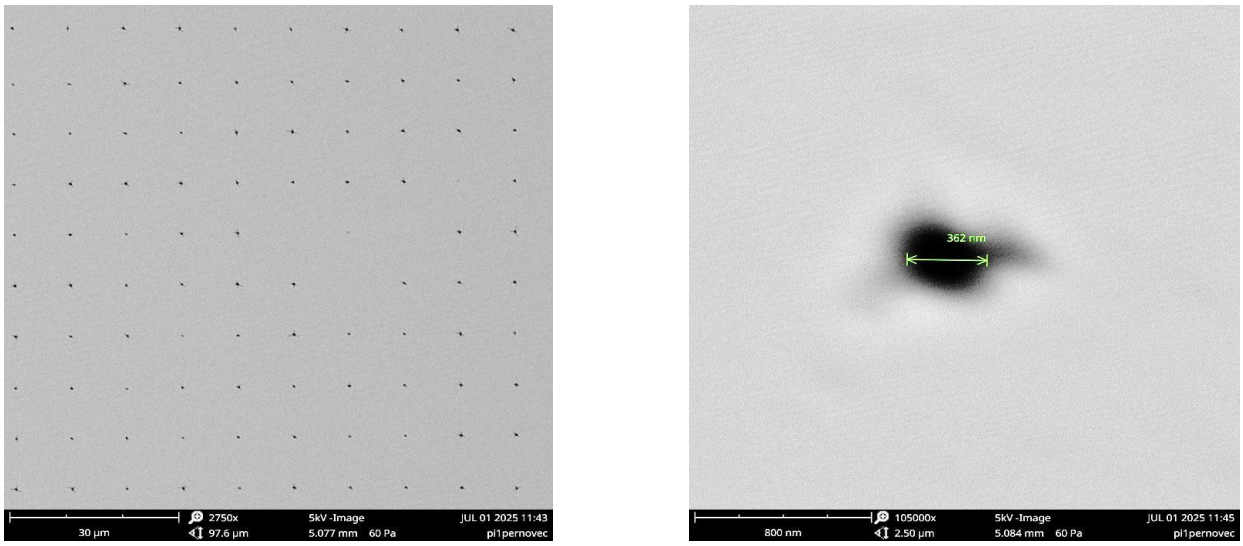

Figure 6 SEM images of pores fabricated within the optimized pulse energy window (20 nJ), scanning speed 1 mm/s, and repetition rate 10 kHz after NaOH etching. Crack-free pores with uniform sub-micrometric diameters (~350 nm) are obtained across the full substrate thickness.

4.3 Influence of repetition rate and scanning speed on crack formation

The influence of repetition rate and scanning speed on pore morphology and crack formation was investigated within the pulse energy range explored in this study. Crack formation was evaluated using a semi-quantitative scoring system based on SEM inspection, assigning scores of 1 to samples exhibiting frequent cracks, 0.5 to samples with few cracks, and 0.1 to samples showing negligible crack formation.

When crack formation is plotted as a function of pulse energy, a clear and monotonic trend is observed, as shown in Figure 7. Low pulse energies (20–30 nJ) consistently result in negligible crack formation, intermediate energies (70–90 nJ) are associated with a moderate crack density, and high pulse energies (≥100 nJ) systematically lead to pronounced crack formation. This energy-dependent behaviour is preserved across the entire range of repetition rates and scanning speeds investigated, indicating that pulse energy is the dominant parameter governing stress-induced defect formation.

To analyze the combined effect of repetition rate and scanning speed, the pulse density along the writing trajectory was defined as the number of laser pulses delivered per unit length:

$$N = \frac{f}{v}$$

where N is the pulse density (pulses/μm), f is the pulse repetition rate, and v is the scanning speed.

When crack formation is plotted as a function of N, no unique or monotonic dependence is observed. Similar crack scores are found over a broad range of pulse densities, indicating that pulse density alone does not fully capture the mechanisms leading to stress accumulation and crack formation. Instead, variations in repetition rate and scanning speed primarily introduce dispersion around the energy-dependent trend rather than shifting it.

Consequently, optimization of crack-free pore fabrication should prioritize pulse energy selection, with repetition rate and scanning speed used as fine-tuning parameters within the energy window identified before.

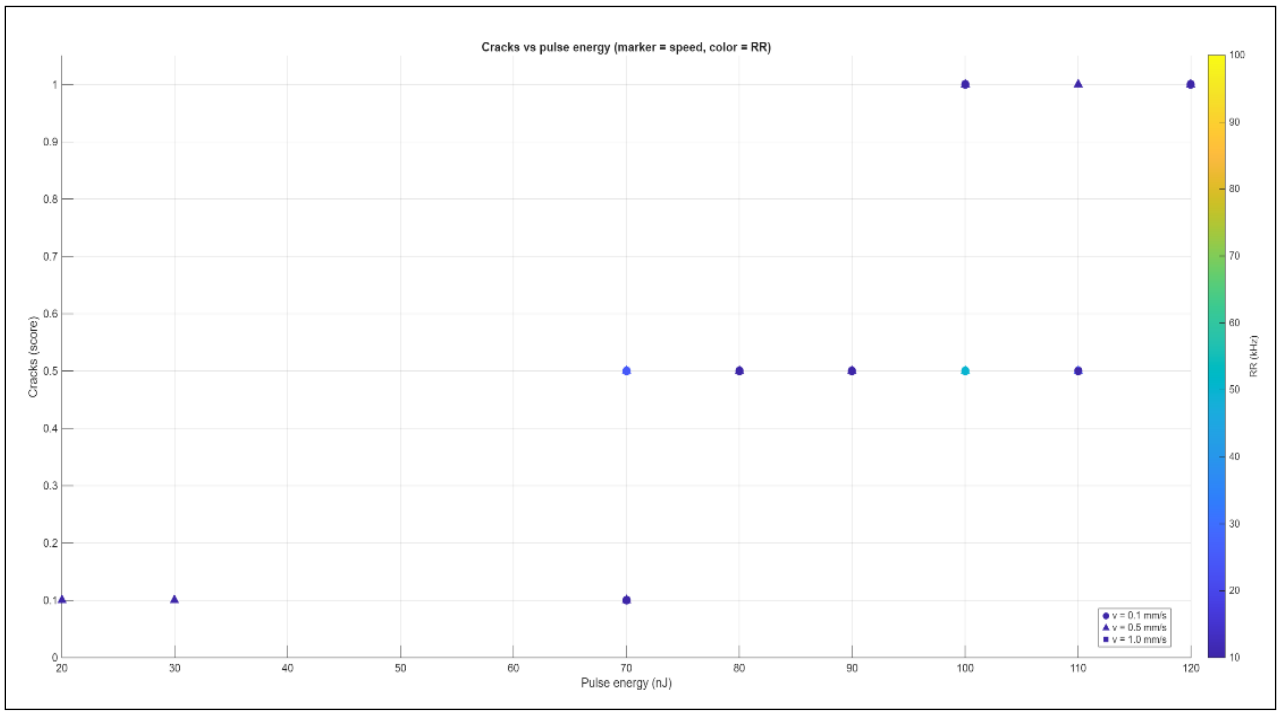

Figure 7 Semi-quantitative crack formation score as a function of laser pulse energy. Crack density decreases monotonically with decreasing pulse energy, identifying an optimal fabrication window between 30 and 20 nJ.

5. CONCLUSIONS

In this work, a laser-fabricated acellular barrier based on nanostructured glass membranes was investigated as a physically defined platform for transport studies relevant to blood–brain barrier (BBB)-on-chip systems. By decoupling physical permeability from biological variability, this approach addresses a key limitation of current BBB-on-chip platforms, where the membrane contribution is often treated as a passive background element rather than an actively engineered subsystem.

Sub-micrometric pores were fabricated in glass substrates using femtosecond-laser selective etching, and the influence of laser writing strategy and irradiation parameters was systematically analyzed. The results show that laser writing geometry affects near-surface integrity and etching accessibility, revealing a trade-off between axial continuity of the laser-modified region and stress accumulation at the glass–water interfaces. Interrupted writing strategies effectively reduce surface damage but require hydrofluoric acid to complete pore opening, whereas continuous axial writing enables full pore penetration using alkaline etching alone when operated within an appropriate energy window.

Among all investigated parameters, pulse energy was identified as the dominant factor governing crack formation, etching uniformity, and final pore morphology. High pulse energies lead to stress-induced cracking, while insufficient energies result in incomplete modification. An optimal fabrication regime was identified at a pulse energy of approximately 20 nJ, where crack formation is strongly suppressed and pores are fully opened by NaOH etching alone. In this regime, the fabricated pores exhibit uniform sub-micrometric diameters of approximately 350 nm across the full 170 µm substrate thickness.

In future work, the permeability of the fabricated glass membranes will be systematically investigated using a dedicated two-chamber setup. Permeability tests will be performed under controlled incubation conditions, introducing a defined oxygen concentration difference between the two chambers to quantify gas transport across the membrane and to better understand the permeability of the laser-fabricated nanoporous structures.

ACKNOWLEDGEMENTS

This work has been supported by the WISE project – *Multi-scale multi-process machine for high value-added complex products with disruptive functionalities*, funded by the European Union's Horizon 2020 research and innovation programme under Grant Agreement No. 101138718.

REFERENCES

[1] L. M. Griep, F. Wolbers, B. de Wagenaar, P. M. ter Braak, B. B. Weksler, I. A. Romero, P.-O. Couraud, I. Vermes, A. D. van der Meer, and A. van den Berg, "BBB on chip: Microfluidic platform to mechanically and biochemically modulate blood–brain barrier function," Biomed. Microdevices, vol. 15, pp. 145–150, 2013.

[2] K.-H. Tu, L.-S. Yu, Z.-H. Sie, H.-Y. Hsu, K. T. Al-Jamal, J. T.-W. Wang, and Y.-Y. Chiang, "Development of real-time transendothelial electrical resistance monitoring for an in vitro blood–brain barrier system," Micromachines, vol. 12, no. 1, p. 37, 2021.

[3] P.-H. Yang, F.-Y. Zheng, Q.-S. Li, T. Tian, G.-Y. Zhang, L. Wu, and H.-J. Mao, “An easy-repeat method to build a blood–brain barrier model on a chip with independent TEER detection module,” Chinese J. Anal. Chem., vol. 50, no. 2, pp. 97–101, 2022.

[4] M. Bonakdar, P. M. Graybill, and R. V. Davalos, “A microfluidic model of the blood–brain barrier to study permeabilization by pulsed electric fields,” RSC Adv., vol. 7, pp. 42811–42818, 2017.

[5] [5] M. Zakharova, M. A. Palma do Carmo, M. W. van der Helm, H. Le-The, M. N. S. de Graaf, V. Orlova, A. van den Berg, A. D. van der Meer, K. Broersen, and L. I. Segerink, “Multiplexed blood–brain barrier organ-on-chip,” Lab Chip, vol. 20, pp. 3132–3143, 2020.

[6] K. Corral-Nájera, G. Chauhan, S. O. Serna-Saldívar, S. O. Martínez-Chapa, and M. M. Aeinehvand, “Polymeric and biological membranes for organ-on-a-chip devices,” Microsyst. Nanoeng., vol. 9, p. 107, 2023.

[7] M. A. Deli, G. Porkoláb, A. Kincses, M. Mészáros, A. Szecskó, A. E. Kocsis, J. P. Vigh, S. Valkai, S. Veszelka, F. R. Walter, and A. Dér, “Lab-on-a-chip models of the blood–brain barrier: Evolution, problems, perspectives,” Lab Chip, vol. 24, pp. 1030–1063, 2024.

[8] E. G. B. M. Bossink, M. Zakharova, D. S. de Bruijn, M. Odijk, and L. I. Segerink, “Measuring barrier function in organ-on-chips with cleanroom-free integration of multiplexable electrodes,” Lab Chip, vol. 21, pp. 2040–2049, 2021.

[9] Y. B. Arık, M. W. van der Helm, M. Odijk, L. I. Segerink, R. Passier, A. van den Berg, and A. D. van der Meer, “Barriers-on-chips: Measurement of barrier function of tissues in organs-on-chips,” Biomicrofluidics, vol. 12, p. 042218, 2018.

[10] M. Odijk, A. D. van der Meer, D. Levner, H. J. Kim, M. W. van der Helm, L. I. Segerink, J.-P. Frimat, G. A. Hamilton, D. E. Ingber, and A. van den Berg, “Measuring direct current trans-epithelial electrical resistance in organ-on-a-chip microsystems,” Lab Chip, vol. 15, pp. 745–752, 2015.